PACS: 52.55.Pi

FIRST ORBIT LOSSES OF CHARGED FUSION PRODUCTS IN TOKAMAK: FLUX CALCULATION

A.O. Moskvitin[1], V.O. Yavorskij[2,3], V.Ya. Goloborod'ko[2,3], Yu.K. Moskvitina[4]

[1] *V.N. Karazin Kharkiv National University*
Ukraine, Kharkiv, Svobody sq. 4, 61022
[2] *Institute for Nuclear Research, Ukrainian Academy of Sciences*
Ukraine, Kyiv, prospekt Nauky b.47, 03680
[3] *Association EURATOM-OEAW, Institute for Theoretical Physics*
Austria, Innsbruck
[4] *National Science Centre "Kharkov Physics and Technology Institute"*
Ukraine, Kharkiv, Akademicheskaya St. 1, 61108
E-mail: Anton.Moskvitin@gmail.com
Received 29 March 2012, accepted 21 May 2012

Technique of calculation the pitch-angle, energy and poloidal distributions of the flux of charged fusion products (CFPs) lost to the first wall of axisymmetric tokamak due to first orbit (FO) loss mechanism is developed. This technique extends the approach for evaluation the poloidal distributions of FO loss of CFPs in tokamaks proposed by [*Kolesnichenko Ya.I. et al. Sov. J. Plasma Phys* ***2*** *(1976) 506*]. The upgraded technique enables to calculate distributions of lost fast ions in wide class of tokamak magnetic configurations. Analytical model of the magnetic field used in this study [*Yavorskij V.A. et al. Plasma Phys. Control. Fusion* ***43*** *(2001) 249*] takes into account Shafranov shift, elongation, triangularity and up-down asymmetry. Usage of the drift constant of motion space allows substantial reducing the computational efforts for simulation the lost particles flux at a given point of the first wall. The developed approach is useful for simulation the pitch-angle and energy distributions of fast ions lost to the scintillator detector [*Zweben S.J. et al. Nucl.Fusion* ***30*** *(1990) 1551*] in present-day tokamaks [*Kiptily V.G. et al. Nucl.Fusion* ***49*** *(2009) 065030*] as well as for calculation of the CFP fluxes to the plasma-facing wall in future tokamak-reactors.
KEYWORDS: first orbit losses, charged fusion product, axisymmetric tokamak, non-circular flux surface, scintillator detector.

МГНОВЕННЫЕ ПОТЕРИ ЗАРЯЖЕННЫХ ПРОДУКТОВ СИНТЕЗА В ТОКАМАКЕ: ВЫЧИСЛЕНИЕ ПОТОКА

А.А. Москвитин[1], В.А. Яворский[2,3], В.Я. Голобородько[2,3], Ю.К. Москвитина[4]

[1] *Харьковский национальный университет имени В.Н. Каразина*
Украина, Харьков, пл. Свободы 4, 61022
[2] *Институт ядерных исследований Национальной академии наук Украины*
Украина, Киев, пр. Науки 47, 03680
[3] *Ассоциация Евроатом-ААН, Институт теоретической физики*
Университет Инсбрука, Австрия
[4] *Национальный научный центр Харьковский физико-технический институт*
Украина, Харьков, ул. Академическая 1, 61108

Разработан метод для расчета распределений по питч-углу, энергии и полоидальному углу потока заряженных продуктов синтеза (ЗПС), теряемых на первой стенке осесимметричного токамака вследствие мгновенных потерь (МП). Этот метод расширяет подход для расчета полоидального распределения МП ЗПС в токамаках, который был предложен в [*Kolesnichenko Ya.I. et al. Sov. J. Plasma Phys* ***2*** *(1976) 506*]. Усовершенствованный метод позволяет рассчитывать распределений теряемых быстрых ионов для широкого класса магнитных конфигураций токамаков. Используемая в этом исследовании аналитическая модель магнитного поля учитывает шафрановский сдвиг, эллиптичность, треугольность и асимметрию «верх-низ» [*Yavorskij V.A. et al. Plasma Phys. Control. Fusion* ***43*** (*2001) 249*]. Использование пространства инвариантов движения дает возможность значительно уменьшить вычислительные усилия при моделировании потока теряемых частиц в заданную точку на первой стенке. Разработанный подход полезен для моделирования распределения по питч-углу и энергии теряемых быстрых ионов, которые попадают в сцинтилляционный детектор [*Zweben S.J. et al. Nucl.Fusion* ***30*** *(1990) 1551*] в современных токамаках [*Kiptily V.G. et al. Nucl.Fusion* ***49*** *(2009) 065030*], а также рассчитывать потоки ЗПС на первую стенку в будущих токамаках реакторах.
КЛЮЧЕВЫЕ СЛОВА: мгновенные потери, заряженные продукты синтеза, осесимметричный токамак, некруглые потоковые поверхности, сцинтилляционный детектор.

МИТТЄВІ ВТРАТИ ЗАРЯДЖЕНИХ ПРОДУКТІВ СИНТЕЗУ В ТОКАМАЦІ: РОЗРАХУНОК ПОТОКУ

А.О. Москвітін[1], В.О. Яворський[2,3], В.Я. Голобородько[2,3], Ю.К. Москвитина[4]

[1] *Харківський національний університет імені В.Н. Каразіна*
Україна Харків, пл. Свободи 4, 61022
[2] *Інститут ядерних досліджень Національної академії наук України*
Україна, Київ, пр. Науки 47, 03680
[3] *Асоціація Євроатом-ААН, Інститут теоретичної фізики*
Університет Інсбрука, Австрія
[4] *Національний науковий центр Харківський фізико-технічний інститут*
Україна, Харків, вул. Академічна 1, 61108

Розроблено метод обчислення розподілів по пітч-куту, енергії та полоїдного куту потоку заряджених продуктів синтезу, які втрачаються на першій стінці осесиметричного токамака внаслідок миттєвих втрат (МВ). Цей метод розширює підхід для обчислення полоїдного розподілу МВ ЗПС в токамаках, який був запропонований в [*Kolesnichenko Ya.I. et al. Sov. J. Plasma Phys* ***2*** *(1976) 506*]. Покращений метод дозволяє розраховувати розподіли швидких іонів, що втрачаються, для широкого класу магнітних конфігурацій токамаків. Аналітична модель магнітного поля, яка використовується в цьому дослідженні, враховує шафранівський зсув, еліптичність, трикутність та асиметрію «верх-низ» [*Yavorskij V.A. et al. Plasma Phys. Control. Fusion* ***43*** *(2001) 249*]. Використання простору інваріантів руху дає можливість значно зменшити обчислювальні зусилля при моделюванні потоку частинок, що втрачаються, в заданій точці на першій стінці. Розроблений підхід є корисним для моделювання розподілу за пітч-кутами та енергіями швидких іонів, що втрачаються, та досягають сцинтиляційного детектора [*Zweben S.J. et al. Nucl.Fusion* ***30*** *(1990) 1551*] у сучасних токамаках [*Kiptily V.G. et al. Nucl.Fusion* ***49*** *(2009) 065030*], а також обчислювати потоки ЗПС на першу стінку в майбутніх токамаках-реакторах.
КЛЮЧОВІ СЛОВА: миттєві втрати, заряджені продукти синтезу, осесиметричний токамак, некруглі потокові поверхні, сцинтиляційний детектор.

Charged fusion product (CFP) losses together with neutron fluxes are expected to cause main damage of a fusion reactor first wall. One of the conventional loss mechanisms of CFP is the first orbit (FO) losses. The thorough review on theoretical study of this loss mechanism is presented in [1]. Review on experimental research activities can be find in [2]. Analytical approaches for first orbit flux calculation were derived in [3,4]. It should be noted that these models were provided for poloidal distributions of FO loss of CFPs in tokamak with circular cross-section. The approach developed in [5] gives an opportunity to calculate the poloidal distribution of FO loss flux in tokamak with elliptic cross-section. The numerical code presented in current study in addition to poloidal distributions allows also examination of pitch-angle and energy distributions of the FO loss in tokamaks with elliptic and triangular flux surfaces.

First systematic experimental research of the FO losses of CFPs was carried out in TFTR (Tokamak Fusion Test Reactor) [6]. The main diagnostic system in this research was the scintillator detector of charged particle. It was able to measure a pitch-angle and energy distribution of the escaped fast ions due to the design of the detector. The scintillator detector is widely used on nowadays tokamaks JET (Joint European Torus) [7,8], ASDEX-Upgrade [9], DIII-D [10] mainly for studying losses of energetic particles caused by either plasma MHD activity, either complex symmetry-breakings [11, 12, 13]. It is assumed that complex symmetry breakings are the magnetic perturbations that break axial symmetry of the tokamak magnetic configuration, e.g. toroidal field ripples, magnetic perturbations caused by Edge Localized Modes (ELMs) mitigation coils, magnetic perturbations caused by Test Blanket Modules in ITER etc. In the framework of these studies, first orbit losses usually cause an unavoidable background signal.

After the first experiments in TFTR, it became obvious that first orbit losses can be decreased significantly due to increasing plasma current above $3MA$, e.g. in ITER with plasma current of order $15MA$ and minor radius $2m$ these losses are believed to be negligibly small (below 0.1%) [11]. Besides that, these experiments showed that these losses are in good agreement with theoretical predictions. Nevertheless, interest to these losses in this study is caused by necessity to develop common approach for simulation of first orbit loss signal in scintillator probe in order to distinguish contributions from the studied processes and from the FO losses. Thus toroidal field ripple induced losses were observed in addition to the conventional first orbit losses of DD CFPs in JET [14].

The crucial point of this study is to use magnetic field model, which could cover variety of the existing tokamak configurations, in order to provide crosscheck for different experimental setups. The appropriate model was developed in [15]. Using this model, it is also possible to carry out test particle simulations using the same numerical model of the magnetic configuration [16].

Description of CFP dynamics needs accurate accounting for the Larmor radius of the orbit. For typical parameters of a reactor scale closed magnetic traps this radius can exceed about 10 cm for CFP. Larmor motion of CFP can be taken into account in the developed approach by appropriate modification of the boundary values of motion invariants. However, to simplify the analysis of FO loss distributions in this paper we neglect the finite Larmor orbit width. Additionally, test particle simulations were carried out using the same magnetic configuration in order to provide a cross-check. The results showed good agreement for 2D smooth profile of the axially symmetric first wall. Nevertheless, the same simulation for real 3D wall will need to take into account the finite Larmor orbit width. Developing of such extended approach is underway now.

Thus, the main aim of this study is to develop the theoretical approach for simulation spatial and velocity distributions of first orbit losses in order to model the scintillator probe signal of pure first orbit losses. This approach should cover variety of existing magnetic configurations, the magnetic field model should be flexible for predictive modeling, and should maintain test particle simulations for crosscheck validation. Smooth, axially symmetric wall is assumed. The finite Larmor orbit width has been neglected yet, in order to introduce the main ideas of developed approach.

In this paper, the theoretical basis of the developed code is presented along with results of the test runs of this code. The test particle validation and comparative analysis of the experimental data is underway now. The rest of the paper is organized in the following way. In the first section, the analytical model of the axisymmetric magnetic configuration is specified. Next section is devoted to the calculation technique of flux density of the first orbit losses,

including flux calculation model, drift orbit equations in terms of constants-of-motion and drift orbit topology analysis. Results of the test runs and concluding remarks are presented in the last section.

MAGNETIC FIELD MODEL

In current study, magnetic configuration of tokamak is assumed to be axisymmetric with non-circular flux surfaces. The analytical model for such configurations is described in details in [15]. It is supposed that flux surfaces are determined by the parametric dependence of the cylindrical coordinates

$$R(\rho,\chi)=R_0+\Delta(\rho)+\rho\cos(\chi), \tag{1}$$

$$Z(\rho,\chi)=Z_{ax}-k(\rho)\rho\sin(\chi)\left[1-\Lambda(\rho)\cos(\chi)\right]^{\alpha}, \tag{2}$$

where R and Z represent the spatial variables of the cylindrical coordinates $\{R,\varphi,Z\}$, ρ and χ represent variables of the new flux-like coordinates $\{\rho,\chi,\varphi\}$ with clear physical meaning, $\Delta(\rho)$, $k(\rho)$ and $\Lambda(\rho)$ are flux surface parameters: the Shafranov's shift, the elongation parameter and the triangularity parameter respectively, and α is a flux surface model parameter, R_0 is vacuum vessel major radius, Z_{ax} is a Z coordinate of the magnetic axis. The physical meaning of $\{\rho,\chi,\varphi\}$ - coordinates can be understood from Fig.1. The coordinate ρ is a flux surface label and its value is equal to distance between the magnetic axis and the flux surface in the equatorial midplane, and χ is the analog of poloidal angle. The angle φ is the toroidal angle, and its value and direction coincide in both coordinate systems $\{R,\varphi,Z\}$ and $\{\rho,\chi,\varphi\}$.

According to used model, the flux surface parameters can be evaluated using expressions

$$\Delta(\rho)=\Delta_e(\rho), \tag{3}$$

$$k(\rho)=k_e(\rho)M\left[1+\left(1-M^2\right)/\alpha\right]^{\alpha}, \tag{4}$$

$$\Lambda(\rho)=\Lambda_e(\rho)M^2/\left(1-M^2+\alpha\right), \tag{5}$$

where $M=1/\sqrt{1-\Lambda_e^2(\rho)}$, $\Delta_e=\Delta_{e0}\left[1-\left(\rho/a_{pl}\right)^2\right]$, $k_e(\rho)=k_{e0}+k_{e1}\left(\rho/a_{pl}\right)^2$, $\Lambda_e(\rho)=\Lambda_{e0}\left(\rho/a_{pl}\right)^2$.

Quantities Δ_e, k_e and Λ_e for each prescribed flux surface can be derived from the geometrical parameters of flux surface shape. The procedure of such derivation is described in [15]. Numerical values of constants a_{pl}, Δ_{e0}, k_{e0}, k_{e1} and Λ_{e0} are presented in Table 1. It should be noted that the explicit form of the expressions (3), (4) and (5) depends on the certain model of the magnetic configuration. Here it is used one of the three analytical models developed in [15]. These models cover the variety of observed flux surface shapes for axisymmetric toroidal magnetic configurations including up-down asymmetry.

The components of the axisymmetric magnetic field in coordinates $\{R,\varphi,Z\}$ are given by

$$B_R=\frac{J\langle Y\rangle}{\sqrt{g}q(\rho)}\frac{\partial R(\rho,\chi)}{\partial\chi}, \tag{6}$$

$$B_\varphi=\frac{J}{R(\rho,\chi)}, \tag{7}$$

$$B_Z=\frac{J\langle Y\rangle}{\sqrt{g}q(\rho)}\frac{\partial Z(\rho,\chi)}{\partial\chi}, \tag{8}$$

where $J=(\mu_0/2\pi)NJ_{TFC}$ total poloidal current parameter, μ_0 magnetic constant, N number of toroidal field coils (TFC), J_{TFC} poloidal current in single TFC, $q(\rho)$ safety factor, $\sqrt{g}$ Jacobian of coordinate system $\{\rho,\chi,\varphi\}$, $Y(\rho,\chi)$ flux surface geometry factor, $\langle\ldots\rangle=\frac{1}{2\pi}\int_0^{2\pi}d\chi\ldots$ denotes the averaging over poloidal angle χ. The explicit expression for $Y(\rho,\chi)$ depends on magnetic configuration analytical model, and can be evaluated using definition

$$Y=\sqrt{g}/R^2. \tag{9}$$

Magnetic configuration calculated using parameters given in Table 1 is in good agreement with typical axisymmetric equilibrium magnetic configuration in JET. These values for the magnetic configuration parameters are used below, if contrary isn't pointed. As an example, flux surfaces calculated using this analytical model are presented in Fig.1.

Table 1.

Parameters of the magnetic configuration analytical model

Parameter name, unit	Parameter value
Vacuum vessel major radius, *m*	$R_0 = 2.89$
Magnetic axis Z coordinate, *m*	$Z_{ax} = 0.323$
Flux surface model parameter	$\alpha = -0.5$
Maximum minor plasma radius in equatorial plane, *m*	$a_{pl} = 0.961$
Magnetic axis Shafranov shift, *m*	$\Delta_0 = 0.11$
Elongation profile parameters	$k_{e0} = 1.36$, $k_{e1} = 0.315$
Triangularity profile parameter	$\Lambda_{e0} = 0.174$
Total poloidal current parameter, *T·m*	$J = -7.58$

MODEL OF THE FLUX OF CFP LOST FROM THE TOKAMAK PLASMA DUE TO THE FO LOSS MECHANISM

Flux calculation model

Commonly total flux of lost particles Γ_{loss} can be written as

$$\Gamma_{loss} = \int\limits_{Loss\ domain} R_{fus}(\mathbf{r},\mathbf{v})\, d\mathbf{r} d\mathbf{v}\,, \tag{10}$$

where $R_{fus}(\mathbf{r},\mathbf{v})$ source of charged fusion product particles, $\mathbf{r}$ and $\mathbf{v}$ radius vector and velocity vector respectively. The integration domain '*Loss domain*' is defined by full set of particle orbits, which intersects confinement boundary, e.g. last closed flux surface or vacuum vessel wall. Here we assume that particle is lost if its trajectory intersects plasma boundary $\rho = a_{pl}$.

Generally, the integration domain is six-dimensional. However, taking into account axial symmetry of the problem and using guiding center approximation, this domain becomes four-dimensional. This means that a full set of lost particle trajectories can be described by only four variables. Thus, the concrete set of four numbers defines only one specific orbit. Certainly, it is true if effect of Coulomb collisions is neglected.

Diagnostic techniques, such as scintillator probe or Faraday cup, give a tip to choose the set of variables in following way $\{a, \chi_a, \xi_a, V\}$, where a, χ_a define the position of probe in $\{\rho, \chi\}$ coordinates, and ξ_a, V describe orbit parameters (pitch $\xi = V_{\|}/V$ and particle speed V, where $V_{\|}$ is parallel particle velocity). Nevertheless, it is possible to derive alternative representation of lost particle flux in terms of variables $\{a, \chi_a, \xi_a, V\}$

$$\Gamma_{loss} = \int\limits_{Loss\ domain} R_{fus}(\rho, \xi_a, V)\sqrt{g}\,\frac{\partial(\rho,\chi,\xi,V)}{\partial(a,\chi_a,\xi_a,V)}\, 2\pi d\rho d\chi_a 2\pi V^2 d\xi_a dV\,, \tag{11}$$

where it is supposed that source of charged fusion product particles R_{fus} in real space depends only on flux label ρ and it is axially symmetric in velocity space regarding to the direction of magnetic field. First assumption is based on the thesis that R_{fus} depends only on plasma specie densities and temperatures, which are commonly supposed to be constant on the flux surface. The second one is a consequence of the fast phase mixing due to cyclotron gyration.

In order to establish relationship between $\{a, \chi_a, \xi_a, V\}$ and $\{\mathbf{r}, \mathbf{v}\}$ variables, and derive the expression for the Jacobian of coordinates transition $\partial(\rho,\chi,\xi,V)/\partial(a,\chi_a,\xi_a,V)$ it is necessary to provide drift orbit analysis.

Drift constants of motion

There are three constants of motion for charged particle in axisymmetric toroidal magnetic field: the total energy $W = mV^2/2$, the magnetic moment $\mu = mV_{\perp}^2/2B$ and the toroidal angular momentum $P_\varphi = R(mV_{\|} - eA_\varphi)$, where m and e are particle mass and electric charge (not necessarily the electron charge), V is particle speed, $V_{\|}$ and $V_{\perp}$ are particle velocity components respectively parallel and perpendicular to the magnetic filed, $\mathbf{B}$, $B = |\mathbf{B}|$, R is radial component of the $\{R, \varphi, Z\}$ cylindrical coordinates, A_φ is a toroidal component of a vector potential $\mathbf{A}$.

Taking into account the invariance of μ and P_φ, guiding center motion equations take the form

$$\left(1-\xi^2\right)R=\left(J/W\right)\mu_a, \tag{12}$$

$$\Psi+\left(mV/e\right)\xi R=P_{\varphi a}/e, \tag{13}$$

where $\left(J/W\right)\mu_a$ and $P_{\varphi a}/e$ are constants, which define certain orbit, subscript $'a'$ points that invariants μ and P_φ are expressed in terms of variables $\mathbf{c}_a=\{\chi_a,\xi_a,V\}$ and $\Psi=-A_\varphi$. Finally, one can get

$$\left(1-\xi^2\right)R(\rho,\chi)=\left(1-\xi_a^2\right)R_a, \tag{14}$$

$$\Psi(\rho)+C\xi R(\rho,\chi)=\Psi_a+C\xi_a R_a, \tag{15}$$

where $R_a=R(a,\chi_a)$, $\Psi_a=\Psi(a)$ and $C=mV/e$. These equations implicitly define particle trajectory $\rho(\chi,\mathbf{c}_a)$ and pitch-angle variation along orbit $\xi(\chi,\mathbf{c}_a)$. Nevertheless, not only χ can be chosen as the independent parameter, it is also possible to consider ρ or ξ as independent variable.

In order to exclude the dependence on χ these equations can be rewritten as

$$R(\rho,\mathbf{c}_a)=\left(B_\xi+D_\xi\right)/2C, \tag{16}$$

$$\xi(\rho)=\left(B_\xi-D_\xi\right)/2A_\xi, \tag{17}$$

where $A_\xi=\Psi(\rho)-\Psi(a)-C\xi_a R_a$, $B_\xi=\left(1-\xi_a^2\right)R_aC$ and $D_\xi=\sqrt{B_\xi^2+4A_\xi^2}$, these designations are made for convenience reasons.

Under given orbit parameters $\{a,\chi_a,\xi_a,V\}$ it is possible to reconstruct the guiding center trajectory for particle with speed V, which passes through point $\{a,\chi_a\}$ with pitch ξ_a. For this purpose, one can change ρ continuously and evaluate R from Eq. (16). Then using R and ρ it is possible to derive χ

$$\chi=\arccos\left\{\left[R(\rho)-R_0-\Delta(\rho)\right]/\rho\right\}. \tag{18}$$

Finally, using Eq. (2) coordinate Z can be obtained.

Examples of reconstructed trajectories are in Fig.2. Taking into account up-down symmetry of magnetic configuration, and supposing that point $\{a,\chi_a\}$ is the final point of trajectory, independent parameter ρ should be changed only in segment $[\rho_{\min},a]$, where $\rho_{\min}$ is value of variable ρ at the point of intersection of trajectory with equatorial midplane (see Fig.2).

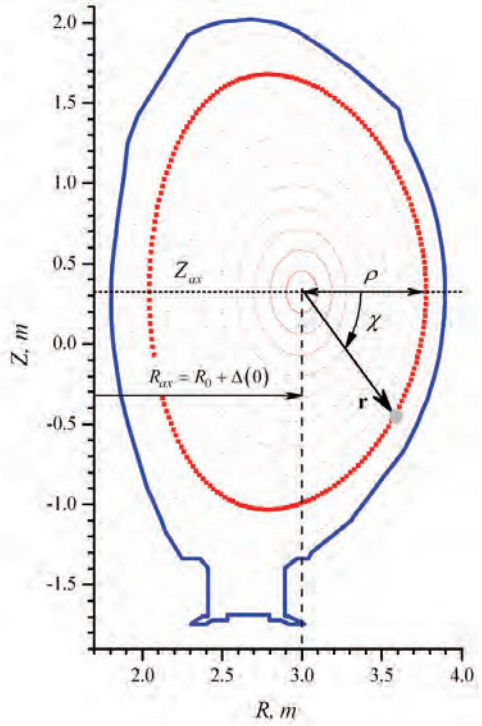

Fig. 1. Flux surfaces, coordinates $\{R,\varphi,Z\}$ and $\{\rho,\chi,\varphi\}$

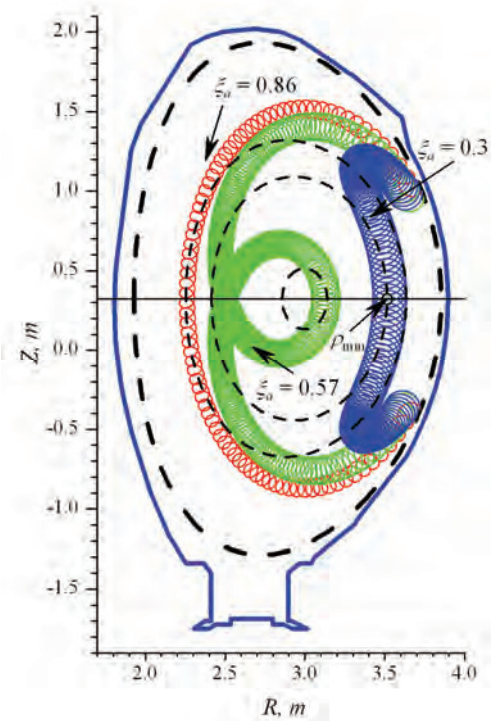

Fig. 2. Typical orbits of charged particles in axisymmetric tokamak configuration .

To find $\rho_{\min}$ one can derive the equation

$$C^2R^2(\rho_{\min},\chi_{\min})-A_\xi^2(\rho_{\min})+B_\xi CR(\rho_{\min},\chi_{\min})=0, \quad (19)$$

where $\chi_{\min}=0$ for intersection point at the '*low field side*' and $\chi_{\min}=\pi$ for the '*high field side*'. Strictly saying, these two types of orbits are separated by the extreme trapped orbit, so called, '*the widest banana orbit*'. It is demonstrated in Fig.2. by bold line. Analysis of the drift orbit topology in axisymmetric magnetic configuration is presented in next subsection.

Drift orbit topology analysis

First of all, let us introduce commonly used charged particle orbits classification: 'co-passing', 'counter-passing' and trapped orbits [17]. Examples of orbits, which reach the detector, are presented in Fig.2 (from left to right): 'co-passing' ($\xi_a=0.86$), 'the fattest banana' ($\xi_a\approx 0.59$), 'banana' ($\xi_a=0.3$). Simulation parameters: tritons with energy $W=1MeV$, probe position $a=0.961m$, $\chi_a=\pi/6$. Dashed lines correspond to flux surfaces, bold dash line represents the outermost flux surface $\rho=a=0.961m$.

In order to give analytical description of the orbit variety and to determine boundaries of the appropriate domains in phase space, we will consider the set of orbits with fixed set of variables $\{a,\chi_a\}$ and we will analyze the position of trajectory intersection point with equatorial midplane $\rho_{\min}$ as a function of parameter values $\{\xi_a,V\}$.

In order to find $\rho_{\min}$ let us consider Eq.(19). In general, this equation doesn't have analytical solution taking into account magnetic configuration considered in this paper. In order to treat this equation numerically it is necessary to localize roots. Dependence of the left hand side of Eq. (19) versus $\rho_{\min}$ for different parameter values $\{\xi_a,V\}$ is presented in Fig.3. For present study, firstly, we are interested in dependence on ξ_a under fixed V. This interest is caused by experimental reasons.

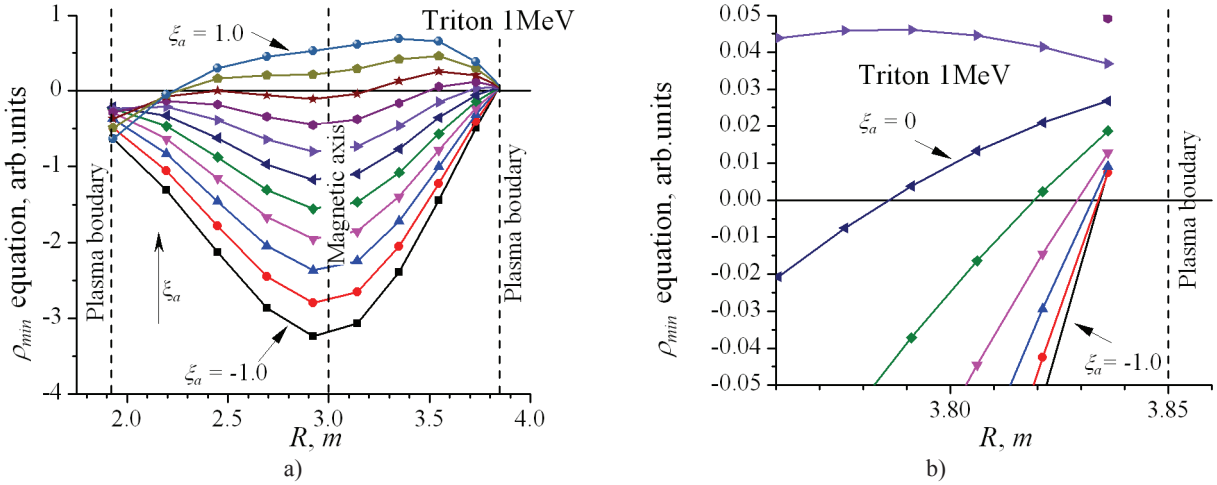

Fig.3. Graph presentation of the LHS of Eq. (19) for $\rho_{\min}$.

a) pitch ξ_a varies from -1 to 1 with step 0.2; b) enlarged fragment of a) for $\xi_a<0$

It is seen from Fig.3b. that for orbits with $\xi_a<0$ only one root for each orbit exists at the 'high field side' near plasma edge. In Fig.2. these orbits lie to the right of orbit with $\xi_a=0$. It is obvious that particles with such trajectories can't give any significant flux at point $\{a,\chi_a\}$, because they pass through plasma periphery with low density. That is why we won't pay attention to these orbits further.

The 'banana' orbits also have only one root. The most problematic are potato orbits, because they have two roots, and these roots don't necessary lie on both sides from magnetic axis. In order to distinguish these roots one should find $\rho_{\min}$ for 'the widest banana' orbit. Further it is denoted as $\rho_{\min}^{wb}$. And ξ_a^{wb} is the value of the orbit invariant ξ_a, which corresponds to the 'widdest banana' orbit. Then two roots of the 'potato orbits' will lie on both sides of $\rho_{\min}^{wb}$. Besides that there is very narrow class of 'twins' orbits. Under '*twins*' here we understand orbits with different set of parameters $\{a,\chi_a,\xi_a,V\}$ but the same coefficients $\{A_\xi,B_\xi,C\}$ and thus the same equation for $\rho_{\min}$. These orbits have three roots: two roots lies at the 'high field side' and one – at the 'low field side'. The leftmost root belongs to 'co-passing' orbit which moves down to point $\{a,\chi_a\}$. And two others belong to closed orbit of 'counter-passing' particle, which

doesn't loss because it doesn't pass through point $\{a,\chi_a\}$. Nevertheless, these orbits can be distinguished too with the help of $\rho_{\min}^{wb}$.

To find $\rho_{\min}^{wb}$ it is necessary to find the root of the first derivative of P_φ. The matter is that the toroidal angular moment under given $\{a,\chi_a,V\}$ has an extremum for 'the widest banana' orbit. Thus it is possible to find ξ_a^{wb} (or corresponding $\rho_{\min}^{wb}$) using equation

$$\frac{\partial\left(P_\varphi/e\right)}{\partial\rho_{eq}}=\frac{2\Psi'\left(\rho_{eq}\right)\xi_{eq}+C\left(1+\xi_{eq}^2\right)R'\left(\rho_{eq},\pi\right)}{2\left(\xi_{eq}-\xi_a\right)}, \tag{20}$$

where 'prime' denotes derivative $d/d\rho_{eq}$ and ρ_{eq} is a coordinate of the intersection point of the drift orbit and equatorial plane, ξ_{eq} is the value of the pitch at the equatorial plane. In fact, variable ρ_{eq} is equal to $\rho_{\min}$ for 'co-passing' and 'the widest banana' orbits, but here it is considered as independent variable, which labels drift orbit. The variables ξ_{eq} and ξ_a in Eq. (20) are functions of ρ_{eq} only. The explicit expressions for $\xi_{eq}\left(\rho_{eq}\right)$ and $\xi_a\left(\rho_{eq}\right)$ can be derived from Eqs. (14) and (15):

$$\xi_{eq}\left(\rho_{eq}\right)=\left(-b_\xi+\sqrt{b_\xi^2-4a_\xi c_\xi}\right)\Big/\left(2a_\xi\right), \tag{21}$$

where $a_\xi=C^2R\left(\rho_{eq},\pi\right)\left[R\left(\rho_{eq},\pi\right)-R_a\right]$, $b_\xi=2CR\left(\rho_{eq},\pi\right)\left[\Psi\left(\rho_{eq}\right)-\Psi_a\right]$ and $c_\xi=C^2R_a\left[R\left(\rho_{eq},\pi\right)-R_a\right]+\left[\Psi\left(\rho_{eq}\right)-\Psi_a\right]^2$; and

$$\xi_a\left(\rho_{eq}\right)=\left(-b'_\xi+\sqrt{b'^2_\xi-4a'_\xi c'_\xi}\right)\Big/\left(2a'_\xi\right), \tag{22}$$

where $a'_\xi=C^2R_a\left[R\left(\rho_{eq},\pi\right)-R_a\right]$, $b'_\xi=2CR_a\left[\Psi\left(\rho_{eq}\right)-\Psi_a\right]$ and $c'_\xi=C^2R\left(\rho_{eq},\pi\right)\left[R\left(\rho_{eq},\pi\right)-R_a\right]-\left[\Psi\left(\rho_{eq}\right)-\Psi_a\right]^2$. It should be noted that all quantities in Eq. (20) - (22) corresponds to equatorial midplane at the 'high-field side'.

The plots of $\xi_a\left(\rho_{eq}\right)$ given by Eq. (22) for different values of the particle energy W are presented in Fig.4. The corresponding orbit types are illustrated in Fig.5 for triton with energy $W=1MeV$. It should be noted that the case $W=2MeV$ in Fig.4 corresponds the situation when all orbits of trapped particles with $\xi_a>0$ are 'potato' orbits.

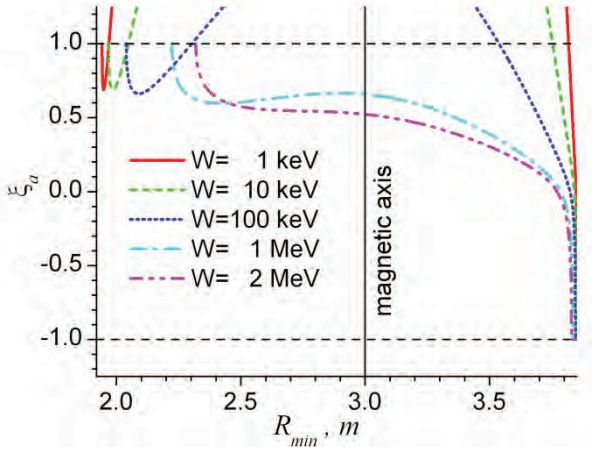

Fig.4. The profile of the orbit parameter ξ_a in equatorial midplane. Simulation parameters: tritons with energies $W=\{1,10,100,1000,2000\}keV$, probe position $a=0.961m$, $\chi_a=\pi/6$.

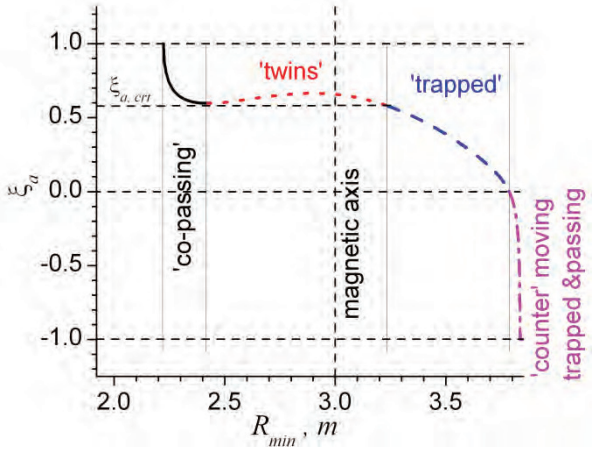

Fig.5. The profile of the orbit parameter ξ_a in equatorial midplane for triton with energy $W=1MeV$, and probe position $a=0.961m$, $\chi_a=\pi/6$.

According to the presented drift orbit analysis it is now possible to localize roots of the Eq. (19) and to finish the definition of '*Loss domain*' in $\{a,\chi_a,\xi_a,V\}$. Thus the expression (11) for the loss particle flux can be written as

$$\Gamma_{loss} = 2\pi \int_{-\pi}^{\pi} d\chi_a \int_0^{\infty} dV 2\pi V^2 \int_{-1}^{1} d\xi_a 2 \int_{\rho_{\min}(a,\chi_a,\xi_a,V)}^{a} d\rho R_{fus}(\rho,\xi_a,V)\sqrt{g}\frac{\partial(\rho,\chi,\xi,V)}{\partial(a,\chi_a,\xi_a,V)}, \quad (23)$$

where $\sqrt{g}$ can be derived using Eqs. (1) and (2), and $\partial(\rho,\chi,\xi,V)/\partial(a,\chi_a,\xi_a,V)$ can be derived using expressions (16) and (17).

RESULTS AND CONCLUSIONS

Commonly, the scintillator probe is placed at the fixed point. This gives an opportunity to consider only flux at the given location $\{a,\chi_a\}$. Next point is that this probe data contains information about separate flux tubes with the given pitch and particle speed $\{\xi_a,V\}$, i.e. the signal from the certain channel of probe is in fact proportional only to value of the integral over ρ in (23). Thus for further study we will consider only monoenergetic flux I of lost particles at point $\{a,\chi_a\}$ with pitch and velocity $\{\xi_a,V\}$

$$I(a,\chi_a,\xi_a,V) = \int_{\rho_{\min}(a,\chi_a,\xi_a,V)}^{a} d\rho R_{fus}(\rho,\xi_a,V)\sqrt{g}\frac{\partial(\rho,\chi,\xi,V)}{\partial(a,\chi_a,\xi_a,V)}. \quad (24)$$

Following expressions for metric coefficients can be used:

$$\sqrt{g} = R^2(\rho,\chi)k(\rho)\rho\tau\{\gamma_0 + \gamma_1\cos\chi + \gamma_2\cos^2\chi + \gamma_3\cos^3\chi\} \quad (25)$$

where coefficients τ and γ_i are given in Table 2 in according with [15];

$$\frac{\partial(\rho,\chi,\xi,V)}{\partial(a,\chi_a,\xi_a,V)} = \frac{a\sin\chi_a}{\rho\sin\chi}\frac{1+\xi_a^2}{1-\xi_a^2}\frac{1}{\sqrt{1+4/G^2}}, \quad (26)$$

where $G = B_\xi / A_\xi$. It is supposed integration along orbit in Eq. (24). Thus, the variable χ in Eqs. (25) and (26) can be derived using Eq. (18)

Table 2.

Magnetic field model coefficients

γ_0	$1+l+\alpha dl$	τ	$(1-\Lambda\cos\chi)^{\alpha-1}$
γ_1	$d-(1+l-\alpha)\Lambda-\alpha m_\Lambda$	d	Δ'
γ_2	$-l-(1+\alpha)dl$	l	$(k'/k)\rho$
γ_3	$(l-\alpha)\Lambda+\alpha m_\Lambda$	m_Λ	$\rho\Lambda'$

To provide numerical integration in Eq. (24) it is used Gauss scheme with 32 points. This scheme doesn't require the evaluation of integrand at the integration domain ends. This feature of the scheme becomes very useful taking into account singularity of Eq. (26) at $\chi = 0$ and $\chi = \pi$, which takes place for $\rho = \rho_{\min}$.

The results of the numerical evaluation of Eq. (24) for tritons with energy $W = \{10,100,1000\}keV$ at different values of pitch ξ_a are presented in Fig.6. For this calculation the source term was supposed monoenergetic

$$R_{fus}(\rho,\xi_a,V) = \frac{1}{2\pi V^2}\delta(V-V_0), \quad (27)$$

where $V_0 = \sqrt{2W/m}$.

From Fig.6 it is obvious that form of flux profile for triton energies $W > 2MeV$ is different compared with triton energies $W < 2MeV$. It is caused by topology of orbits with large energy, namely, orbits of all 'trapped' particles are 'potato', and there are no 'banana' orbits (see Fig.4). Besides that, there is no 'gap' in the equatorial midplane, which corresponds to 'twins' orbits (see Fig.5).

It is obvious that FLR effects play significant role in the CFP dynamics. However, to simplify the analysis of FO loss distributions in this paper we neglect the finite Larmor orbit width. Nevertheless, gyro-orbit simulation of 400000 test particles was carried out using in order to provide a cross-check. The results of this calculation are demonstrated in Fig. 7. It is seen that distributions of both approaches are in reasonable agreement.

In test simulation particles were uniformly distributed in the torus RZ-section bounded by last closed flux surface. Each particle was traced for 20 microseconds; it corresponds to nearly 2000 cyclotron periods of triton in this magnetic configuration. All parameters of magnetic configuration were the same as provided above in the paper. The error bars of points, which correspond to 'full orbit' calculations, are estimated using expression for dispersion of the binomial distribution.

$$f_{Err}(\xi_{ai}) = \sqrt{N_\Sigma p_i (1-p_i)}, \quad (28)$$

where f_{Err} notes absolute magnitude of the error for point ξ_{ai}, N_Σ is total number of particles escaping to the scintillator probe with pitch $\xi_a > 1$, p_i is the probability that $\xi_{ai} - \Delta\xi/2 < \xi_a < \xi_{ai} + \Delta\xi/2$, $(\Delta\xi = 0.05)$.

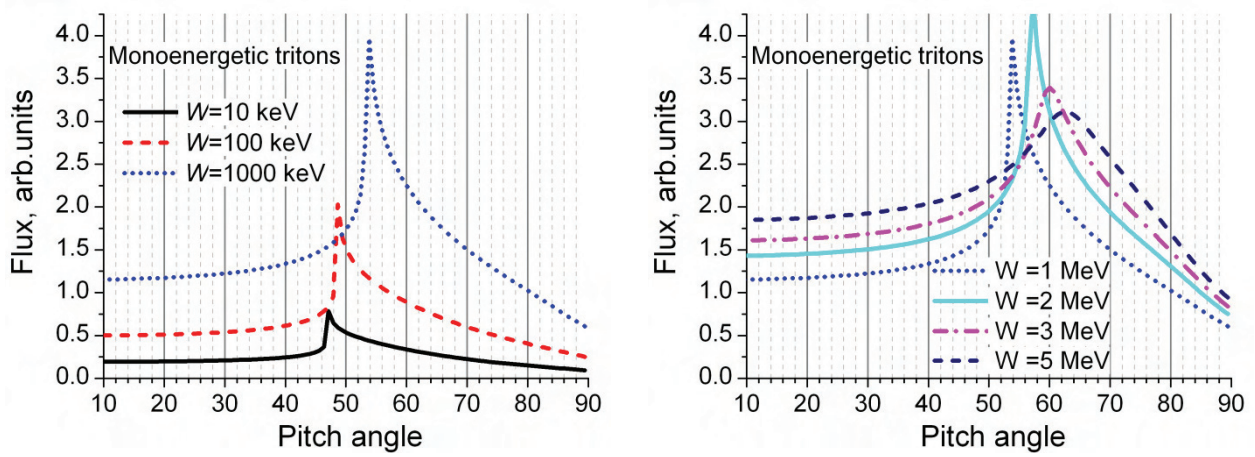

Fig.6. Fluxes of lost tritons with monoenergetic distribution
a) $W = \{10,100,1000\} keV$; b) $W = \{1,2,3,5\} MeV$.

The mean deviation of models σ is estimated as

$$\sigma = \sqrt{\left(f_{full\,orbit}(\xi_i) - f_{drift}(\xi_i)\right)^2 / N}, \quad (29)$$

where $f_{full\,orbit}$ and f_{drift} are values of normalized flux at point with pitch ξ_i, N is a number of points $(N = 20)$.

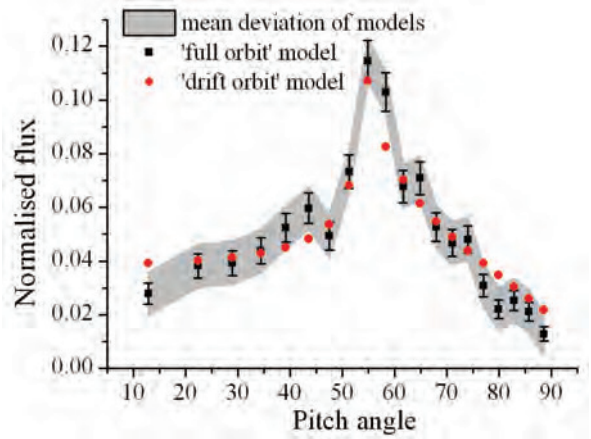

Fig. 7. Comparison of the pitch angle distribution of the lost CFP, which are calculated using 'full orbit' and 'drift orbit' models. The error bars are estimated using Eq. (28).

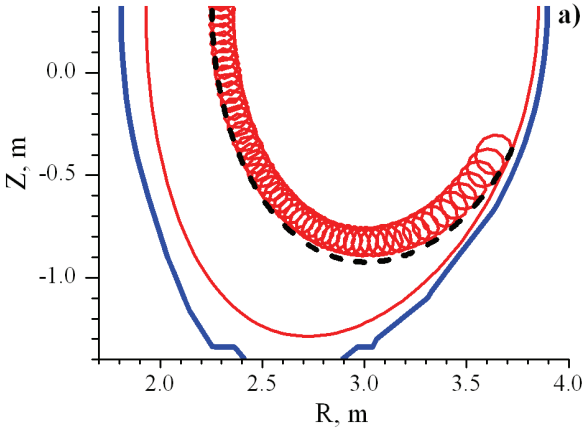

Fig. 8. Comparison of the lost trajectories, which are calculated using 'full orbit' (solid line) and 'drift orbit' (dash line) models. a) $\xi_a = 0.725$ (pitch angle ~ 40^0);

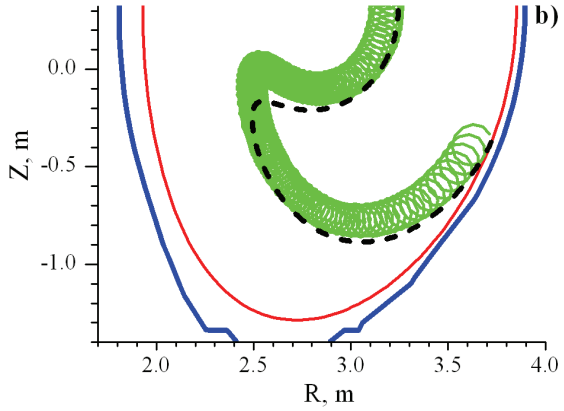

Fig. 8.(cont.) b) $\xi_a = 0.575$ (pitch angle ~ 55^0);

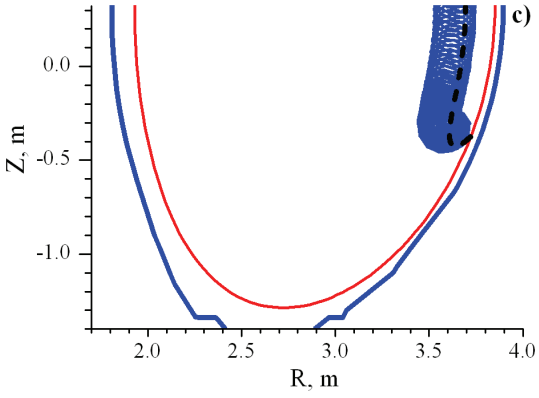

Fig. 8.(cont.) c) $\xi_a = 0.175$ (pitch angle ~ 80^0);

To clarify the nature of the discrepancies of FO loss distributions in Fig. 7 we compare the drift and full gyro orbits for circulating and toroidally trapped particles considered in this figure. Fig. 8a represents the trajectories of the passing particle with pitch $\xi_a = 0.725$ (pitch angle ~ 40^0), while Figs. 8b and 8c display the orbits of toroidally trapped particles with $\xi_a = 0.575$ (pitch angle ~ 55^0) and $\xi_a = 0.175$ (pitch angle close to 80^0). One can see that for circulating particle the length of the 'drift' trajectory is greater than the length of its guiding center trajectory in the 'full orbit' model. Contrary the lengths of drift orbits of trapped particles are less than those of the guiding centers of full gyro-orbits. The biggest deviation in orbit lengths is observed for trapped particle with pitch angle ~ 55^0 (Fig. 8b) that can explain the underestimation of the FO loss of marginally trapped particles at pitch angles 55-60^0 in drift approximation seen in Fig. 7.

In order to clarify the effect of energy profile of the source term, numerical simulation was provided for 'Gauss'-like form

$$R_{fus}(\rho,\xi_a,V) = \frac{mV}{2W_{CM}}\sqrt{\frac{\gamma}{\pi}}\exp\left\{-\gamma\left[\sqrt{\frac{W}{W_{CM}}}-1\right]^2\right\}, \qquad (30)$$

where $W = mV^2/2$, $\gamma = W_{CM}/\beta T$, W_{CM} is birth energy in center mass frame, β is distribution dispersion parameter, T is plasma temperature. Examples of distributions given by Eq.(30) are presented in Fig.9.

Numerical simulations show that the energy distribution of fusion product affects weakly on the pitch distribution of the flux. As an example, calculated pitch distributions are presented in Fig.10 for the cases of monoenergetic and 'Gauss'-like of the fusion product energy distribution. It is caused mainly by weak dependence of the critical value of pitch for *'the widest banana'* orbit on energy (see Fig.4).

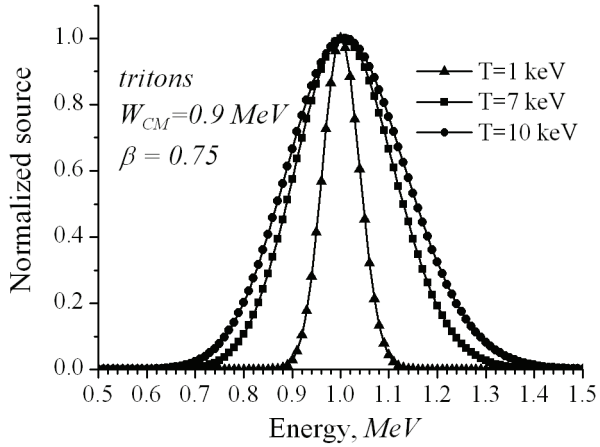

Fig.9. Energy spectra of the fusion product triton source for plasma temperatures $T = \{1,7,10\}keV$.

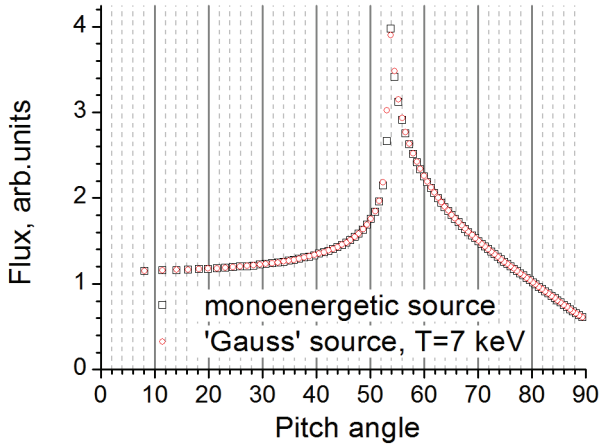

Fig.10. Lost triton flux profile for different forms of the source term.

In conclusion, we would like to summarize main results of the presented study. The earlier developed approach for poloidal distribution of prompt losses of CFP is extended to calculate pitch-angle and velocity distributions of the lost ions. The numerical code for simulation of the first orbit losses of CFP is developed for axisymmetric magnetic configuration of tokamak taking into account non-circular flux surfaces. Smooth axially symmetric 2D wall is assumed I this model. Cross-check of the newly upgraded approach against full orbit calculations shows good agreement.

Drift orbit topology analysis in this configuration is provided in order to define the '*Loss domain'* in constants of motion space. The approach used in this paper gives an opportunity to decrease calculation efforts for simulating the experimental data from scintillator probe, or other point probe. It is shown that the energy spectrum of the charged fusion product weakly affects the lost particles flux profile versus pitch. Results of the test numerical simulation agree with earlier conducted calculations [3-5] and experimental data [14].

REFERENCES

1. Kolesnichenko Ya.I. The role of alpha particles in tokamak reactors // Nuclear Fusion. – 1980. – Vol.20, № 6. – P. 727 - 780.
2. Heidbrink W.W., Sadler G.J. The behaviour of fast ions in tokamak experiments // Nuclear Fusion. – 1994. – Vol.34, № 4. – P. 535-615.
3. Kolesnichenko Ya.I., Fursa A.D., Yavorskiy V.A. Azimutal'noe raspredelenie potoka vysokoenergichnykh al'fa-chastits na stenki kamery v aksial'no-simmetrichnom tokamake // Fizika plazmy. – 1976. – T.2, vyp. 6. – S. 911 - 921. (in Russian). Kolesnichenko Ya.I., Fursa A.D., Yavorskij V.A. Azimuthal distribution of the flux of high-energy alpha-particles to the chamber wall in an axisymmetric tokamak // Soviet Journal of Plasma Physics. – 1976. – Vol.2, № 6. – P. 506-510. (in English).

4. Hively L.M., Miley G.H. Fusion product bombardment of a tokamak first wall // Nuclear Fusion. – 1977. – Vol.17, № 5. – P. 1031 - 1046.
5. Kolesnichenko Ya.I., Yavorskiy V.A. Ob uderzhanii al'fa-chastits v tokamakakh s nekruglym secheniem // Fizika plazmy. – 1979. – T.5, Vyp. 1. – C. 126 – 135 (in Russian). Kolesnichenko Ya.I., Yavorskij V.A. Alpha-particle confinement in a tokamak with a noncircular cross section // Soviet Journal of Plasma Physics. – 1979. – Vol.5, № 1. – P. 72-77. (in English).
6. Zweben S.J., Boivin R.L., Diesso M. et al. Loss of Alpha-Like MeV Fusion Products from TFTR // Nuclear Fusion. – 1990. – Vol.30, № 8. – P. 1551-1574.
7. Kiptily V.G., Borba D., Cecil F.E. et al. Fast ion JET diagnostics: confinement and losses // AIP Conference Proceedings **988**, Burning Plasma Diagnostics: An International Conference, Varenna, Italy, September 24-28. – 2007. Abstract Booklet. – P. 283-290.
8. Baeumel S., Werner A., Semler R. et al. Design of lost alpha particle diagnostics for JET // Fusion Enginnering and Design. – 2005. – Vol.74. – P. 853-857.
9. Garcia-Munoz M., Fahrbach H.-U., Zohm H. et al. Scintillator based detector for fast-ion losses induced by magnetohydrodynamic instabilities in the ASDEX upgrade tokamak // Review of Scientific Instruments. – 2009. – Vol.80, № 5. – P. 053503 (1-9).
10. Fisher R.K., Pace D.C., García-Munoz M. et al. Scintillator-based diagnostic for fast ion loss measurements on DIII-D // Review of Scientific Instruments. – 2010. – Vol.81, № 10. – P. 10D307 (1-3).
11. ITER Physics Expert Group on Energetic Particles, ITER Physics Basis Editors, ITER EDA et al. Chapter 5: Physics of Energetic Ions // Nuclear Fusion. – 1999. – Vol.39, № 12. – P. 2471-2495.
12. Fasoli A., Gormenzano C., Berk H.L. et al. Chapter 5: Physics of Energetic Ions // Nuclear Fusion. – 2007. – Vol.47, № 6. – P. S264-S284.
13. Shinohara K., Kurki-Suonio T., Spong D. et al. Effects of complex symmetry-breakings on alpha particle power loads on first wall structures and equilibrium in ITER // Nuclear Fusion. – 2011. – Vol.51, № 6. – P. 063028 (1-12).
14. Baranov Yu., Jenkins I., Kiptily V. et al. Evidence of anomalous losses of fusion products on JET // 37th EPS Conference on Plasma Physics, Dublin, Ireland, June 21 - 25. – 2010. – P5.141.
15. Yavorskij V.A., Schoepf K., Andrushchenko Zh.N. et al. Analytical models of axisymmetric toroidal magnetic fields with non-circular flux surfaces // Plasma Physics and Controlled Fusion. – 2001. – Vol.43, № 3. – P. 249 - 269.
16. Yavorskij V., Baranov Yu., Goloborod'ko V. et al. Modelling of spatial and velocity distributions of diffusive fast ion loss in JET // 38th EPS Conf. on Plasma Phys., Strasbourg, France, June 27 – July 1. – 2011. – P4.029.
17. Rome J.A., Peng Y-K.M. The topology of tokamak orbits // Nuclear Fusion – 1979. – Vol.19, №.9. – P. 1193-1205.